

PACS numbers: 42.55.Ks; 42.60.Lh; 42.65.Re
DOI: 10.1070/QE2001v031n07ABEH002014

Numerical simulation of the active medium and investigation of the pump source for the development of a photochemical XeF($C-A$) amplifier of femtosecond optical pulses

G Ya Malinovskii, S B Mamaev, L D Mikheev, T Yu Moskalev,
M L Sentis, V I Cheremiskin, V I Yalovoi

***Abstract*. Numerical simulations of the active medium of an XeF($C-A$) amplifier were used to determine the conditions for its spatially uniform excitation. It is shown that in the transient regime of the bleaching wave formation, the excitation efficiency increases with increasing steepness of the pump pulse leading edge. An optical source for pumping an XeF($C-A$) amplifier was developed and investigated. The source is based on a radically new approach to the production of a large-area surface discharge (of the order of 100 cm^2 and over) without using switches in the feed circuit connected in series with the discharge. Radiation pulses of the shortest duration (0.6 – 0.7 μs) for this kind of sources were obtained. There are grounds to believe that applying this source in a 50-cm long multipass amplifier will provide an overall gain of $\sim 10^3$.**

Keywords: *numerical stimulation, active medium, pump source, photochemical XeF amplifier, femtosecond pulses*

1. Introduction

An XeF active medium in which the $C-A$ transition is used for lasing has long been discussed in the scientific literature as an alternative to the existing systems for the amplification of femtosecond optical pulses. An advantage of this transition is its broad ($\sim$ 60 nm) spectrum in the 480-nm region, which is equivalent to the spectra of $\sim$ 10-fs transform-limited pulses, and a high, as compared to other excimers employed, saturation energy density of 0.05 J cm^{-2}. Another favourable feature of this transition is the coincidence of its wavelength with the second harmonic of a Ti : sapphire laser, which significantly simplifies the formation of the pulse being amplified.

Finally, this medium is a gas with a density of about 10^{19} cm^{-3} and therefore allows a direct pulse amplification without using the chirped-pulse technique, which involves employment of complex and costly systems for the stretching and compression of the pulses being amplified. The latter circumstance becomes especially important at high output powers approaching 10^{15} W.

Moreover, the gaseous nature of the medium allows its scaling. At present, output energies of a photochemical XeF laser of the order of 1 kJ in the UV range (on the $B-X$ transition) [1] and 120 J (on the $C-A$ transition) [2] were experimentally obtained.

The possibility to amplify femtosecond optical pulses on the XeF($C-A$) transition casts no doubt. This is confirmed by the results of experimental studies of the amplification of 800- and 250-fs pulses on this transition to a terawatt power with electron-beam pumping [3, 4] and by the theoretical analysis of amplification of pulses with durations down to 50 fs [5]. The approach proposed in our work is different only in that the method of producing the active medium is more simple and inexpensive. This method involves the photodissociation of XeF_2 vapour by vacuum UV (VUV) radiation (145 – 180 nm) [6].

A specific feature of excitation of the existing XeF lasers is the formation of a bleaching wave, which is responsible for the occurrence of a narrow active region running away from the pump source. The bleaching wave and the related excitation wave are formed because the lifetime of XeF_2 molecules in the radiation field of the pump source $(\sigma I)^{-1}$ near its surface proves to be significantly shorter than the excitation pulse ($\sim 10^{-5} - 10^{-4}$ s) due to the high XeF_2 absorption cross section ($\sigma_{max} \sim 7 \times 10^{-17}$ cm^2 at the maximum of the absorption band at $\lambda_{max} = 158$ nm) and the photon flux into the absorption band ($I \sim 10^{23}$ photon × cm^{-2} s^{-1}). This results in a total dissociation of the substance not only within a layer of unit optical thickness adjacent to the pump source, but also in deeper optical layers. As a consequence, in the absorbing medium a bleaching wave emerges at the front of which the active medium is excited. These processes were considered in greater detail in several papers (see, for instance, Refs [7 – 14] and references therein).

A technique of femtosecond optical pulse amplification in the bleaching wave was proposed in Ref. [15]. We will consider a somewhat different principle, which involves a spatially uniform excitation of the active medium due to partial photodecomposition of XeF_2. This proves to be possible in the initial period of bleaching wave production (during the transient regime) in the active medium placed between two plane pump sources for a unit optical thickness of the absorbing layer comparable with the distance between the sources.

G Ya Malinovskii, S B Mamaev, L D Mikheev, T Yu Moskalev, V I Cheremiskin, V I Yalovoi P N Lebedev Physics Institute, Russian Academy of Sciences, Leninskii prospekt 53, 119991 Moscow, Russia; tel./fax: (095)135 87 03; e-mail: mikheev@sci.lebedev.ru
M L Sentis Laboratoire Lasers, Plasmas et Procedes Photoniques, FRE 2165 CNRS – Aix-Marseille II University, Campus de Luminy, case 917, 13288 Marseille Cedex 09, France

Received 29 January 2001; revision received 23 May 2001
Kvantovaya Elektronika **31** (7) 617 – 622 (2001)
Translated by E N Ragozin

The key problem in the amplifier design is the development of a pump source, which determines the configuration and the properties of the amplifier. The requirements imposed on the amplifier in this case are different from those imposed on electric-discharge pump sources previously employed in photochemical lasers [16]. In particular, a plane pump-source geometry and a submicrosecond radiation pulse rise time are preferable. The plane source geometry facilitates the realisation of a multipass amplification scheme, while shortening the pulse rise time increases the gain, as follows from the numerical analysis of the active medium.

The above requirements are easiest to satisfy by using a surface discharge. The properties closest to those required are inherent in a sheet discharge over a dielectric surface, which is characterised by a large radiant surface (100 cm^2 and over), a radiance temperature of 20 kK and higher, and a strong steepness of the pump pulse edge (see, for instance, Refs [17, 18]). In Refs [17, 18], sheet discharges with an area up to 440 cm^2 were studied. It was shown that the plasma temperature reached 20 kK for specific energies (per unit area of the discharge-covered surface) of over 4 J cm^{-2} [17].

However, the radiation pulse duration under the conditions providing the required specific energy deposition over a large surface are, as a rule, greater than 1 μs. In our opinion, a substantial contribution to the impedance of the discharge circuit is made by the switch connected in series in the feed circuit to produce a sheet-type surface discharge. This switch is required to provide the field strength across the discharge gap that significantly exceeds the breakdown threshold, which is important for the development of a surface-uniform discharge. In addition, the surface sheet discharge is usually characterised by a very low impedance, and therefore the presence of a switching device in the circuit impairs the discharge–power supply matching, which determines the efficiency of a pump source as a whole.

In Ref. [19], a submicrosecond source was described involving a multichannel surface discharge with a plane geometry switched by additional electrodes located in the central part of the discharge gaps. This technique does not necessitate an additional switch connected in series to the main discharge, which permits reducing the impedance of the feed circuit and, accordingly, shortening the pulse to a fraction of a microsecond. Here, we developed a somewhat different principle of the formation of a multichannel surface discharge, which also does not require a switch connected in series.

2. Numerical simulation of the active medium

As already noted, the physical principle of optical excitation of the XeF($C-A$) transition involves the photolysis of XeF_2 by 145–180-nm radiation, resulting in the production of XeF primarily in the B state (the yield of the C state is lower by more than an order of magnitude [20, 21]). With a proper buffer gas, there occurs an efficient collisional relaxation of XeF(B) to the C state lying lower than the B state by approximately 600 cm^{-1}. The working transition is a transition in the blue–green region (480 nm) to the repulsive A state. It is significant that the C state can be efficiently populated only at a relatively low pressure of the buffer gas – of the order of 100 Torr. This circumstance is extremely important because the employment of so tenuous a medium gives grounds to believe that nonlinear effects in the amplifying medium will exert a relatively small influence on the amplification.

Numerical simulations were performed for an active medium placed between two pump sources, which were infinite parallel planes spaced at 3 cm. The temporal profile of the radiation intensity was modelled by a Gaussian curve

$$I = I_{\max} \exp\left[\frac{-(t-t_{\max})^2 4\ln 2}{t_{\max}^2}\right].$$

Here, $I_{\max} = 1.13 \times 10^{23}$ photons cm^{-2} s^{-1} is the maximum intensity corresponding to a radiance temperature of 20 kK, which is attained at the moment $t_{\max}$. As shown below, this temperature estimate is fully justified. The pump source was treated as a blackbody whose brightness is, as is well known, independent of the angle with respect to the radiating surface.

The characteristics of the active medium consisting of xenon difluoride vapour in the atmosphere of argon buffer gas were calculated taking into account the real spectral dependences of XeF_2 absorption cross section and the quantum yield of excited XeF molecules in the 145–180-nm spectral region. The calculations involved the exact numerical solution of radiation transfer and absorbing-particle balance eq-uations, as well as of the system of kinetic equations

$$\cos\theta \frac{\partial I_\lambda}{\partial x} = -\sigma(\lambda) I_\lambda N, \tag{1}$$

$$\frac{\partial N}{\partial t} = -2\pi N \int_{\lambda_1}^{\lambda_2} \int_0^{\pi/2} \sigma(\lambda) I_\lambda \sin\theta \mathrm{d}\theta \mathrm{d}\lambda, \tag{2}$$

$$\frac{\partial B(x,t)}{\partial t} = -\tau_B^{-1} B + k_{CB}^{\mathrm{Ar}} CM + \gamma_B(\lambda) W(x,t), \tag{3}$$

$$\frac{\partial C(x,t)}{\partial t} = k_{BC}^{\mathrm{Ar}} BM - \tau_C^{-1} C + \gamma_C(\lambda) W(x,t). \tag{4}$$

Here, θ is the angle between the beam propagation direction and the normal to the surface $x = 0$ of the pump source; $I_\lambda = I_\lambda(x,t,\boldsymbol{\omega})$ is the spectral intensity of light in the direction of vector $\boldsymbol{\omega}$ at point x; λ is the radiation wavelength; $\sigma(\lambda)$ is the spectral dependence of the absorption cross section for XeF_2 molecules; $N = N(x,t)$, B, C, and M are the concentrations of XeF_2, XeF(B), XeF(C), and Ar molecules, respectively; $W(x,t)$ is the number of photolysis events per unit volume per unit time; γ_B and γ_C are the XeF(B)- and XeF(C)-production quantum yields; k_{BC}^{Ar} and k_{CB}^{Ar} are the rate constants for XeF($B \to C$) collisional relaxation and its reverse process, respectivily; $\tau_B^{-1} = \tau_{BX}^{-1} + S_B + k_{BC}^{\mathrm{Ar}} BM$, $\tau_C^{-1} = \tau_{CA}^{-1} + S_C + k_{CB}^{\mathrm{Ar}} CM$; τ_{BX}^{-1} and τ_{CA}^{-1} are the spontaneous radiative XeF($B \to X$) and XeF($C \to A$) transition probabilities; $S_B = \sum_i k_{Bi} R_i$ and $S_C = \sum_i k_{Ci} R_i$ are the probabilities of XeF(B) and XeF(C) quenching by the mixture components and the photolysis products; and R_i, k_{Bi}, and k_{Ci} are the corresponding concentrations and rate constants. The concentrations of Xe and F atoms are defined by the expression [Xe] = [F]/2 = $N_0 - N$. The initial and boundary conditions are $N(x, t = 0) = N_0$, $I_\lambda(x = 0) = I_\lambda^0(t)$.

The most reliable values of the rate constants for the processes included in the model are presented in Table 1. A more detailed discussion of the kinetic processes in the active medium of a photochemical XeF($C-A$) laser can be found in Refs [6, 13, 25]. The issue of XeF(B)-production

yield in the photolysis of XeF_2 is under discussion to the present day. The maximum values of this yield in the wavelength region under study reported in the literature range from 0.3 to 1 (see Ref. [6] and references therein, and also Ref. [22]). In this paper, the quantum yield was assumed to be equal to unity at the maximum of the spectral dependence because, with this value of the quantum yield, according to Ref. [6], this kinetic model provides the most precise description of the experimentally observed characteristics of the XeF($C-A$) laser. The radiative lifetimes of the XeF(C) and XeF(B) states are 100 and 14 ns, respectively (see, for instance, Ref. [20]).

Table 1. Rates constants (in $cm^3\ s^{-1}$) for the reactions XeF(B) + R → products (k_B^R), XeF(B) + Ar → XeF(C) + Ar(k_{BC}^{Ar}) for $k_{BC}^{Ar}/k_{CB}^{Ar} = 35$, and XeF($C$) + R → products ($k_C^R$).

$k_B^{XeF_2}$	k_B^{Xe}	k_B^{Ar}	k_{BC}^{Ar}	$k_C^{XeF_2}$	k_C^{Xe}	k_C^{Ar}	k_C^{F}
5×10^{-10}	1.5×10^{-11}	5×10^{-14}	8.6×10^{-12}	2×10^{-10}	2×10^{-11}	5×10^{-14}	1.1×10^{-9}
[21]	[23]	[23]	[23]	[23]	[23]	[23]	[24]

The calculations were performed for different initial concentrations of XeF_2 and t_{max}. Fig. 1 shows the results of numerical calculations for a pump pulse with $t_{max} = 0.7$ μs, which coincides, as will be shown below (Fig. 8), in duration and shape with the radiation pulse obtained experimentally when investigating the pump source prototype. One can see that a partial photodecomposition of the initial substance in the active volume leads to its nonuniform spatial distribution, resulting in the establishment of the maximum gain by the time $t = 400$ ns, which is uniform over the cross section (Fig. 1a). In this case, the relative nonuniformity of the gain does not exceed 2 % within the limit of the amplifier aperture. The results of numerical experiments for different distances between the pump sources in the $d = 1 - 10$ cm range show that the degree of uniformity of the gain and the moment at which it achieves its maximum remain virtually unchanged if the initial XeF_2 density varies proportionally to d^{-1}.

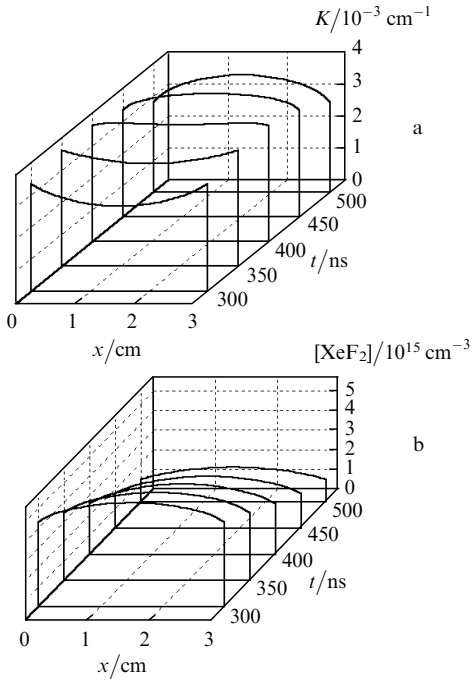

Figure 1. Spatiotemporal distribution of the gain (a) and XeF_2 density (b) at the cross section of the amplifier for initial densities $[XeF_2] = 7.5\times10^{15}$ cm^{-3} and $[Ar] = 2.5\times10^{19}$ cm^{-3}.

Parametric optimisation of the active medium from the viewpoint of spatially uniform amplification of an optical pulse calls for a consideration of the optical amplification scheme with the inclusion of beam divergence. The low gain of the active medium ($\sim 3\times10^{-3}$ cm^{-1}) requires the use of a multipass amplification scheme. We considered an 'optical trap'-type configuration shown in Fig. 2. The pulse being amplified enters the active medium at a small angle β to the optical axis. After sequential reflections from the tilted mirrors, the beam reaches the opposite end of the trap and comes back.

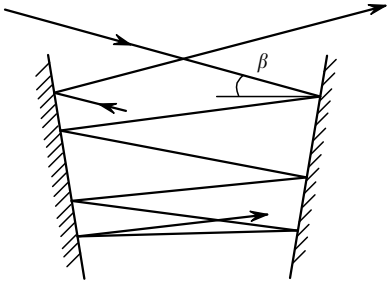

Figure 2. Schematic of optical amplification.

The calculations show that it is possible to realise about 60 passes through an active medium measuring 3 cm× 10 cm ×50 cm for an initial beam diameter of 3 mm and a beam divergence two times the diffraction-limited divergence. In this case, the amplification time amounts to 10^{-7} s, during which the active medium undergoes significant changes. As shown by the calculations, it is nevertheless possible to select the time of injection of the amplified beam in such a way that the beam would remain in the domain of a spatially uniform gain for all time. This is illustrated in Fig. 3, in which curve *1* depicts the time dependence of the width of the domain characterised by a gain nonuniformity of 1 % and curve *2* – the time dependence of the diameter of the beam being amplified with the initial diameter of 3 mm and two times the diffraction-limited divergence. During the 100-ns time interval considered, which corresponds to 60 passes through the active medium, the beam expanded to 1.5 cm, the whole time remaining in the domain with the gain nonuniformity of less than 1 %. As shown by numerical

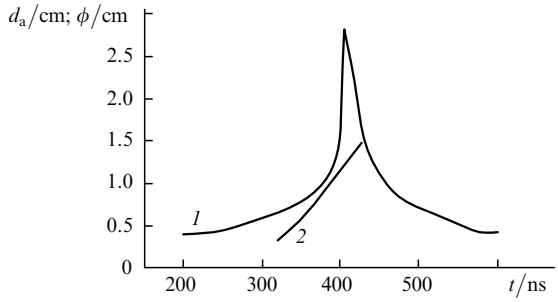

Figure 3. Width of the amplification region d_a with a gain nonuniformity of 1 % (*1*) and beam diameter (*2*) as functions of time. The initial parameters of the pump and the active medium are the same as in Fig. 1.

calculations, the overall small-signal gain in this case can be as high as $\sim 5 \times 10^4$.

It is significant that the optimal conditions for amplification are formed at the leading edge of the pump pulse and, as revealed by numerical simulations for pump pulses with different t_{max}, essentially depend on the steepness of the leading edge of a pulse. The results are given in Fig. 4, which shows the growth of the gain with increasing steepness of the pump pulse edge (with a reduction of t_{max}).

The following two conclusions can be drawn from the results of numerical simulations. First, it is possible to prepare a spatially uniform active medium in an optically thick absorbing medium ($kd \sim 1$, where k and d are the absorption coefficient and the lateral medium dimension, respectively), which provides the most complete utilisation of the pump energy. Second, the amplifier operation efficiency improves as the pump pulse becomes more steep. The latter circumstance imposes stringent requirements upon the design of the pump source: its feed circuit should possess the lowest possible inductance, which determines the current pulse build-up rate.

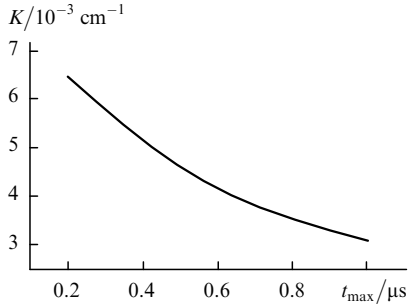

Figure 4. Dependence of the maximum gain on t_{max}. The initial composition of the active medium is the same as in Fig. 1.

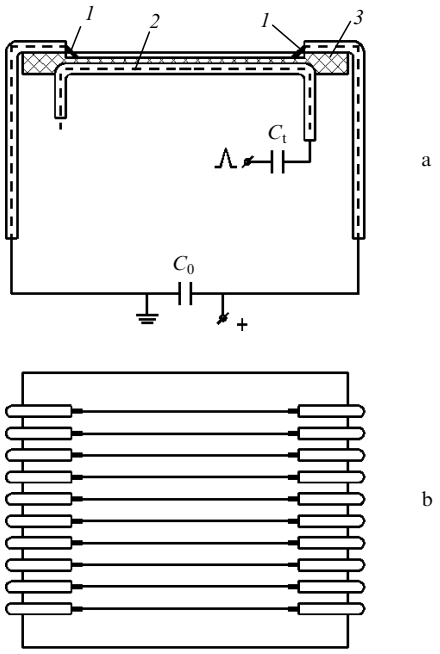

Figure 5. Schematic representation of the pump source involving a multichannel surface discharge [side (a) and top (b) views]: (*1*) discharge electrodes; (*2*) ignitor; (*3*) Teflon substrate.

3. Pump source

To satisfy the above requirements, we designed a pump source based on a multichannel surface discharge whose initiation circuit is shown in Fig. 5. Isolated conductors, which serve as ignitor electrodes, are located at regular intervals of 5 mm on the back side of a Teflon substrate. To improve the linear discharge stabilisation, 1-mm deep grooves are made on the substrate face opposite to the conductors. The discharge gap between the main electrodes is 10 – 11 cm. The electrodes are connected to a storage capacitor with a capacitance $C_t = 0.6$ μF charged to a voltage of 10 – 20 kV. A discharge is initiated by applying a voltage pulse with an amplitude of 20 – 30 kV to the ignitors. As this takes place, in the grooves on the substrate face there occurs a weak barrier discharge induced by displacement currents in the distributed capacitance of the dielectric. The barrier discharge closes the electrode gaps, giving rise to self-sustained discharges along the channels between the main electrodes.

The source was placed in an organic glass housing which was evacuated and filled with an $Ar-N_2$ mixture for a total pressure of 1 bar typical of an $XeF(C-A)$ laser. The $Ar:N_2$ ratio depends on the voltage and ranges from 1:14 to 1:7 in the 10 – 20 kV interval under investigation. The discharge current and voltage were measured with the aid of a calibrated Rogowski loop and an ohmic divider, respectively. The temporal UV-radiation profile was measured with a photodiode. The spatiotemporal discharge uniformity was monitored employing a fast photochronograph with a rotating mirror or a CCD camera. Here, we studied a prototype of the pump source involving a 15-channel discharge with an electrode separation of 10 cm fed by a Maxwell low-inductance capacitor with a capacitance of 0.6 μF and an inductance of 20 nH.

Fig. 6 shows typical pulse shapes of the UV-radiation (in the 370 – 390 nm band) of the surface discharge and current oscilloscope traces obtained with the first prototype for an initial voltage across the capacitor $U_0 = 10$, 15, and 20 kV. The obtained durations of the optical pulse and current period were two times shorter than was the case with initiation of a sheet surface discharge with the aid of a gap [17] for comparable discharge feed energies. Moreover, it follows from the current pulse shape for all experiments described here that the discharge is close to the critical one. This is indicative of a far better feed circuit – discharge matching in comparison with the sheet surface discharge [17]. As U_0 increases, the duration of the first half-cycle shortens from 1.2 μs (for 10 kV) to 1.0 μs (for 20 kV).

The total inductance L and resistance R of the discharge circuit estimated on the basis of the elementary theory of circuits using the resultant oscilloscope traces lie respectively in the 140 – 150 nH and 0.3 – 0.4 Ω ranges ($U_0 = 10 - 20$ kV). Estimates of the electric energy deposited in the discharge made by the formula $E(t) = \int_0^t JU\mathrm{d}t$ show that about 75 % of the energy stored in the capacitor (120 J) is deposited in the course of the first half-cycle. Here, J and are respectively the current and the voltage across the discharge gap measured employing the Rogowski loop and the voltage divider.

The streak-camera photographs of the discharge reveal a rather uniform and simultaneous development of discharges

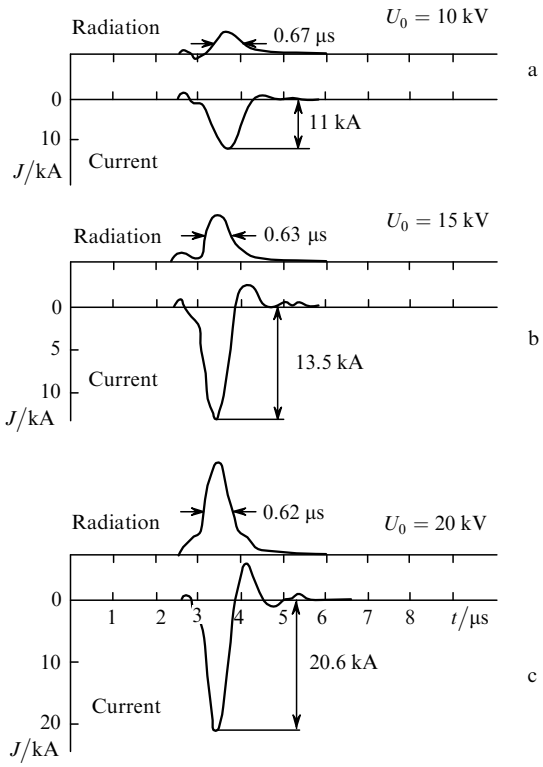

Figure 6. Typical pulse shapes of current and the 370–390 nm UV radiation of the surface discharge for different U_0.

in the channels for all voltages in the 10–20 kV range under study (Fig. 7). This is facilitated by the circumstance that the impedance modulus of discharge in this configuration far exceeds the corresponding value for the feed circuit, and the discharge development in an individual channel does not result in a significant voltage fall in other channels.

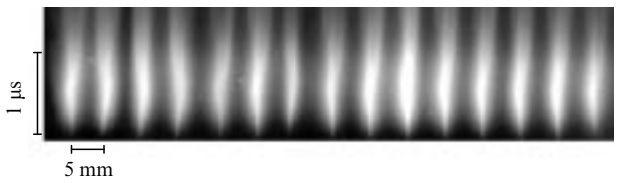

Figure 7. Streak-camera photograph of a 15-channel surface discharge for $U_0 = 20$ kV.

The diameter of an individual plasma channel corresponding to the first current peak for $U_0 = 20$ kV was measured from a streak photograph and was found to be ~ 0.2 cm. Therefore, for 1 cm^2 of the surface occupied by the plasma there are ~ 4 J of energy, and the specific energy per unit plasma volume amounts to ~ 20 J cm^{-3}. These values are comparable with the pertinent values realised in Ref. [17] for a sheet surface discharge which afforded a plasma temperature of about 20 kK. At the same time, note that the electric-energy deposition rate in our case is at least two times that for the sheet discharge.

The results obtained in the studies of the prototype outlined above underlie the design of one of the pump source modules of a photochemical XeF($C - A$) amplifier. The module measuring 11 cm × 25.5 cm differed from the prototype in only that it was designed to employ three storage capacitors of the IKCh-25-0.6 type (0.6 μF capacitance, 15 nH inductance), each loaded with 17 channels (51 channels in all). The electrode separation was 11 cm.

Fig. 8 shows typical time profiles of the current and the 370–390-nm UV radiation power of a surface discharge obtained in the mixture of composition $N_2 : Ar = 1 : 14$ for a total pressure of 1 bar and an initial voltage $U_0 = 15$ kV. The light pulse and current parameters are close to the values obtained in the investigation of the 15-channel discharge. The inductance of the discharge circuit measured from the oscilloscope traces of current with the electrodes short-circuited by conductors 1 mm in diameter was found to be equal to 0.1 μH, which is nearly three times lower than for a sheet surface discharge investigated in Ref. [17]. A discharge photograph obtained with a CCD camera (Fig. 9) demonstrates a rather high uniformity of discharge development in individual channels and allows a conclusion that scaling the multichannel discharge is possible in the context of the above-outlined approach by increasing the number of channels and capacitors.

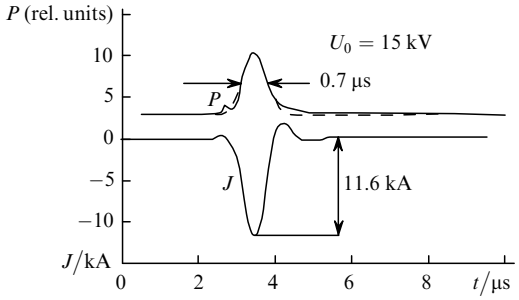

Figure 8. Typical time profiles of the 370–390 nm UV radiation power P and the surface discharge current J for $U_0 = 15$ kV. The approximation of the pulse by a Gaussian function is indicated by the dashed line.

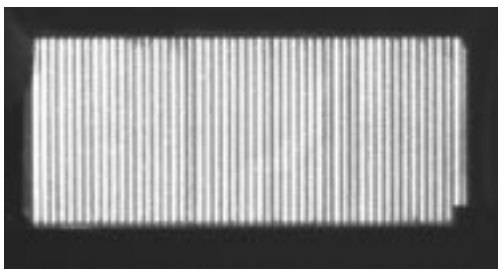

Figure 9. Photograph of a 51-channel discharge made with a 200-ns exposure at the instant of the first current peak.

In the preceding Section we considered a numerical model of the active medium excited by a plane pump source. This model may be employed to describe the time evolution of length-averaged parameters of the active medium excited by the radiation of a multichannel discharge. In this case, the amplitude of the pump pulse should be lowered to take into account the spatial filling factor of the discharge channels. The spatiotemporal dependences of the gain and the density of the initial material thus obtained are accurate replicas of the results given in Fig. 1, though on a different time scale and for a different scale of the gain. The gain to be expected is $(2-2.5)\times 10^{-3}$ cm^{-1}, which gives promise that an overall amplification factor of the order of 10^3 may be attained in 60 passes through a 50-cm long amplifier.

4. Conclusions

Numerical simulations of the active medium have allowed an understanding of the specific features of its behaviour in the transient pumping mode and enabled us to formulate the basic requirements imposed on the optical excitation source and the composition of the active medium to ensure the most efficient and spatially uniform amplification. The spatial uniformity of the gain is due to the partial bleaching of the XeF_2 molecules. For a XeF_2 densities of the order of 10^{16} cm^{-3}, the nonuniformity of the gain at the lateral section of the amplified beam is within 1 %. All other factors being equal, the gain essentially depends on the pump pulse build-up rate, making the development of new submicrosecond pump sources a topical problem.

The method proposed for the production of a multichannel surface discharge with the aid of a barrier discharge without resorting to switches in the discharge circuit is highly fruitful for the development of submicrosecond radiation sources with a large (virtually unlimited) area. Using this approach, we developed a pump source with pulses of 0.6–0.7 μs duration, which is the shortest for large-area (tens of square centimetres) plasma sources with a large specific energy deposition (of the order of 1 J cm^{-2} and over). The source design permits its use as one of the moduli for assembling radiant surfaces of arbitrary area. The source elaborated satisfies the requirements imposed on an XeF($C - A$) amplifier of femtosecond optical pulses. The principle that underlies the source design can be employed for the development of the pump sources for other optically excited lasers, for the preionisation of electric-discharge lasers or the realisation of a plasma cathode, as well as for the solution of other problems neces-sitating high-intensity radiation sources. The studies of the operating characteristics of the pump source demonstrate its long service life: over 10^3 discharges across the Teflon substrate did not result in a noticeable damage of its surface.

Acknowledgements. The authors are grateful to A A Malinovskaya and V V Mislavskii for their assistance and to V S Zuev for fruitful discussions. This work was supported by the INTAS (Grant No. INTAS-97-1869).

References

1. Anisimov S V, Zemskov E M, Zuev V S, Kazanskii V M, Kashnikov G N, Mikheev L D, Nesterov R O, Sokolov V V, Stavrovskii D B, Tcheremiskine V I *Laser Phys.* **4** 416 (1994)
2. Zuev V S, Kashnikov G N, Mamaev S B *Kvantovaya Elektron.* **19** 1047 (1992) [*Sov. J. Quantum Electron.* **22** 973 (1992)]
3. Sharp T E, Hofman T, Dane C B, Wilson W L, Tittel F K, Wisoff P J, Szabo G *Opt. Lett.* **15** 1461 (1990)
4. Hofman Th, Sharp T E, Dane C B, Wisoff P J, Wilson W L, Tittel F K, Szabo G *IEEE J. Quantum Electron.* **28** 1366 (1992)
5. Kannari F *Jap. J. Appl. Phys.* **31** 2109 (1992)
6. Mikheev L D, Stavrovskii D B, Zuev V S *J. Russ. Laser Res.* **16** 427 (1995)
7. Borovich B L, Zuev V S, Katulin V A, Nosach O Yu, Tyurin E L, Shcheglov V A *Kvantovaya Elektron.* (2/8) 88 (1972) [*Sov. J. Quantum Electron.* **2** 160 (1972)]
8. Borovich B L, Zuev V S, Krokhin O N *Zh. Eksp. Teor. Fiz.* **64** 1184 (1973)
9. Zuev V S, Katulin V A *Kvantovaya Elektron.* **24** 1105 (1997) [*Quantum Electron.* **27** 1073 (1997)]
10. Cohen J S, Judd O P *Phys. Rev. A* **27** 3146 (1983)
11. Cohen J S, Judd O P *J. Appl. Phys.* **55** 2659 (1984)
12. Beverly III R E *Appl. Phys. B* **56** 147 (1993)
13. Tcheremiskine V I *Thesis for Ph D (Phys)* (Marseille: Universite de la Mediterranee/Moscow: Moscow Institute of Physics and Technology, 1999)
14. Tcheremiskine V I, Mikheev L D, Sentis M L, Zuev V S *Opt. Lett.* **26** 408 (2001)
15. Mikheev L D *Laser Part. Beams* **10** 473 (1992)
16. Zuev V S, Mikheev L D *Photochemical Lasers* (Chur: Harwood, 1991)
17. Beverly III R E *J. Appl. Phys.* **60** 104 (1986)
18. Baranov V Yu, Borisov V M, Vysikailo F I, Khristoforov O B *Teplofiz. Vys. Temp.* **22** 661 (1984)
19. Tcheremiskine V I, Sentis M L, Delaporte Ph C, Mikheev L D, Zuev V S *Proceedings of the XXIII International Conference on Phenomena in Ionized Gases, Toulouse, France, 1997* Vol. IV, p. 52
20. Black G, Sharpless R L, Lorents D C, Huestis D L, Gutchek R A, Bonifield T D, Helm D A, Walters G K *J. Chem. Phys.* **75** 4840 (1982)
21. Bibinov N K, Vinogradov I P, Mikheev L D, Stavrovskii D B *Kvantovaya Elektron.* **8** 1945 (1981) [*Sov. J. Quantum Electron.* **11** 1178 (1981)]
22. Kono M, Shobatake K *J. Chem. Phys.* **102** 5966 (1995)
23. Brashears H C, Setser D W *J. Chem. Phys.* **76** 4932 (1982)
24. Bishel W K, Eckstrom D J, Walker H C, Jr, Tilton R A *J. Appl. Phys.* **52** 4429 (1981)
25. Cheremiskin V I, Malinovski G Y, Mikheev L D *Preprint No. 7* (Moscow: Lebedev Physics Institute, Russian Academy of Sciences, 1994)